Coordination Cages

International Edition: DOI: 10.1002/anie.201603907
German Edition: DOI: 10.1002/ange.201603907

A Mixed-Ligand Approach for a Gigantic and Hollow Heterometallic Cage $\{Ni_{64}RE_{96}\}$ for Gas Separation and Magnetic Cooling Applications

*Wei-Peng Chen[+], Pei-Qin Liao[+], Youzhu Yu, Zhiping Zheng, Xiao-Ming Chen, and Yan-Zhen Zheng**

Dedicated to Professor Thomas C. W. Mak on the occasion of his 80th birthday

Abstract: *Nanosized aggregations of metal ions shielded by organic ligands possessing both exquisite structural aesthetics and intriguing properties are fundamentally interesting. Three isostructural gigantic transition-metal–rare-earth heterometallic coordination cages are reported, abbreviated as $\{Ni_{64}RE_{96}\}$ (RE = Gd, Dy, and Y) and obtained by a mixed-ligand approach, each possessing a cuboidal framework made of 160 metal ions and a nanosized spherical cavity in the center. Along with the structural novelty, these hollow cages show highly selective adsorptions for CO_2 over CH_4 or N_2 at ambient temperatures. Moreover, the gadolinium analogue exhibits large magnetocaloric effect at ultralow temperatures.*

Polymetallic complexes featuring ordered arrangement of the constituent metal centers into cluster-like core structures are an interesting class of coordination compounds. Early interest in such species originated from the synthetic challenges and their appealing molecular structures.[1–7] The research has now been extended beyond the initial prerogative of synthetic and structural chemistry into materials preparation and property investigation, largely due to the potential in developing molecule-based magnetic materials. Although numerous such compounds have been reported, some of which possessing both exquisite structural beauty and intriguing properties,[8,9] synthetic chemists have been pushing the envelope to assemble even larger species with ever increasing metal nuclearity, while materials scientists are stimulated by the anticipated structure–property correlation in these nanoscopic yet molecular materials as well as the possibility of connecting well-defined molecular systems with any hierarchically assembled nanostructures.

We have been interested in the synthetic and materials chemistry of polymetallic complexes. By controlling the hydrolysis of the metal ions using certain organic ligands, we have obtained a large number of polynuclear transition-rare earth complexes.[10] We found that both the metal and the hydrolysis-limiting ligands are important in determining the nuclearity of the cluster complexes and their specific molecular structures. Attempting at further advancing the synthetic frontiers of such compounds, we recently explored the use of mixed sets of ligands. It is hypothesized that the subtle balance between different ligands may lead to clusters with structures and/or properties that have yet to be envisioned. Herein, we report our preliminary findings with the combined use of iminodiacetic acid (IDA) and 2,2-dimethylol propionic acid (DMPA) to control the co-hydrolysis of mixed Ni^{II} and rare-earth metal RE(III) (RE = Gd, Dy, or Y) ions under solvothermal conditions.

IDA was chosen because of its established success in the assembly of heterometallic 3d–4f complexes.[11] In these complexes, individual complex units of transition-metal ions with IDA are linked through carboxylate O atoms to form a shell of transition-metal complex that formally serves to limit lanthanide hydrolysis; this controlled hydrolysis affords polyhedral lanthanide–hydroxo cores of the eventual heterometallic cluster complexes. Considering the high oxophilicity of the lanthanide ions, we submit that introducing ligands whose coordination is based on the exclusive presence of O atoms may interfere with the coordination of the hydrolytically produced hydroxo groups. As such, both the RE–O core motif and the overall cluster structure are altered. DMPA, a ligand with only O-based coordinating ability, was chosen in this particular capacity.

As verification of this mixed-ligand approach, we report herein three isostructural cluster complexes with common formula of $[Ni_{64}RE_{96}(\mu_3\text{-}OH)_{156}(IDA)_{66}(DMPA)_{12}(CH_3COO)_{48}(NO_3)_{24}(H_2O)_{64}]\ Cl_{24}\cdot x\,CH_3OH\cdot y\,H_2O$ (RE = Gd **1**, $x = 35$, $y = 120$; Dy **2**, $x = 30$, $y = 80$; Y **3**, $x = 8$, $y = 90$) (see Supporting Information for details of synthesis and characterization). To our best knowledge, these giant clusters, possessing a unique porous cube-like structure as revealed by crystallographic studies (see below), represent the highest-nuclearity heterometallic cluster complexes that contain both transition-metal and rare-earth elements. Interestingly, the porous solids of these compounds also exhibit high selectivity

[*] W.-P. Chen,[+] Y. Yu, Prof. Dr. Y.-Z. Zheng
Frontier Institute of Science and Technology (FIST)
State Key Laboratory of Mechanical Behavior for Materials
Xi'an Jiaotong University, Xi'an 710054 (China)
E-mail: zheng.yanzhen@xjtu.edu.cn
Homepage: http://gr.xjtu.edu.cn/web/zheng.yanzhen/home
P.-Q. Liao,[+] Prof. Dr. X.-M. Chen
MOE Key Laboratory of Bioinorganic and Synthetic Chemistry
School of Chemistry and Chemical Engineering
Sun Yat-Sen University, Guangzhou 510275 (China)
Prof. Dr. Z. Zheng
Department of Chemistry, The University of Arizona
Tucson, AZ 85721 (USA)
[+] These authors contributed equally to this work.
Supporting information for this article can be found under: http://dx.doi.org/10.1002/anie.201603907.

for CO_2 over CH_4 or N_2 at room temperature and large magnetocaloric effects (MCEs) at ultralow temperatures.

A structural description of **1** as a representative is given below.[12] The complex cation is a cube-like unit of $[Ni_{60}Gd_{96}(\mu_3\text{-}OH)_{156}(IDA)_{60}(DMPA)_{12}(CH_3COO)_{48}(NO_3)_{24}(H_2O)_{52}]^{24+}$ (abbreviated as $\{Ni_{60}Gd_{96}\}$ hereafter) with four add-on fragments of $\{Ni(IDA)(H_2O)_3\}$ via coordination by the O atoms of IDA ligands (Figure 1; Supporting Information, Figure S1). As anticipated, the DMPA ligand participates in the coordination of the Gd-hydroxo cluster core. It is the "interfering" coordination of this second organic ligand (with respect to IDA) that provides the key linkage between the "propeller-like" $\{Ni_6Gd_9\}$ building block on each vertex of the cuboidal cage and the triangular $\{NiGd_2\}$ units that are located in the middle of the edges. The DMPA ligands are obviously key to preventing the inward expansion of the Gd–hydroxo cluster core with 24 chelating acetate ligands that entrenched in the inside of the inorganic–hydroxo skeleton. Thus, the unique intracluster aperture is formed. Moreover, the shape and the functions of DMPA ligands are like geckos that firmly grasp the metal–hydroxo pillars with the remainder 24 chelating acetate ligands, which ensure a highly stabilized arch structure together, while for the NO_3^- ions, they are symmetrically straggled in the six windows of the hollow cavity to satisfy coordination requirement of Gd ions and balance the charge.

The vertex-building $\{Ni_6Gd_9\}$ unit with approximately a threefold axial symmetry can be viewed as assembled from a $\{Gd_9\}$ sub-core of nine edge-sharing truncated $\{Gd_3O_3(\mu_3\text{-}OH)\}$ cubanes and a triangular $\{Ni_6\}$ subunit of six $\{Ni(IDA)(H_2O)_3\}$ fragments (Figure 1c). Each Ni^{II} ion is situated in a distorted octahedral coordination sphere and every IDA ligand, along with chelating one Ni^{II} ion in a tridentate fashion, adopts the *syn-anti* bridging mode to connect adjacent Ni^{II} ions with a $Ni^{II}\cdots Ni^{II}$ separation of 5.21–5.24 Å (Supporting Information, Figure S2). Such bridged units are then linked with $\{Gd_9\}$ core through triply bridging hydroxo groups and carboxylate O atoms of the IDA ligands to give the vertex-occupying $\{Ni_6Gd_9\}$ unit; eight such units are further connected by 12 units of $\{NiGd_2\}$ to afford an unprecedented $\{Ni_{60}Gd_{96}\}$ cuboidal cage (Figure 1). Alternatively, the cube-like core may be viewed as being formed by using a coordination framework of Ni-IDA to limit the hydrolysis of Gd^{III} to produce the $\{Gd_{96}\}$ core (Supporting Information, Figures S3 and S4).

The nanoscopic cage has an inner cavity of ca. 1.4 nm in diameter with the external edge ca. 3.2 nm (Figure 1d; Supporting Information, Figure S1b). Adjacent clusters are piled up into a 3D extended structure whose porous structure is composed of two kinds of cavities, A and B (Figure 2; Supporting Information, Figures S5 and S6). Cavity A pos-

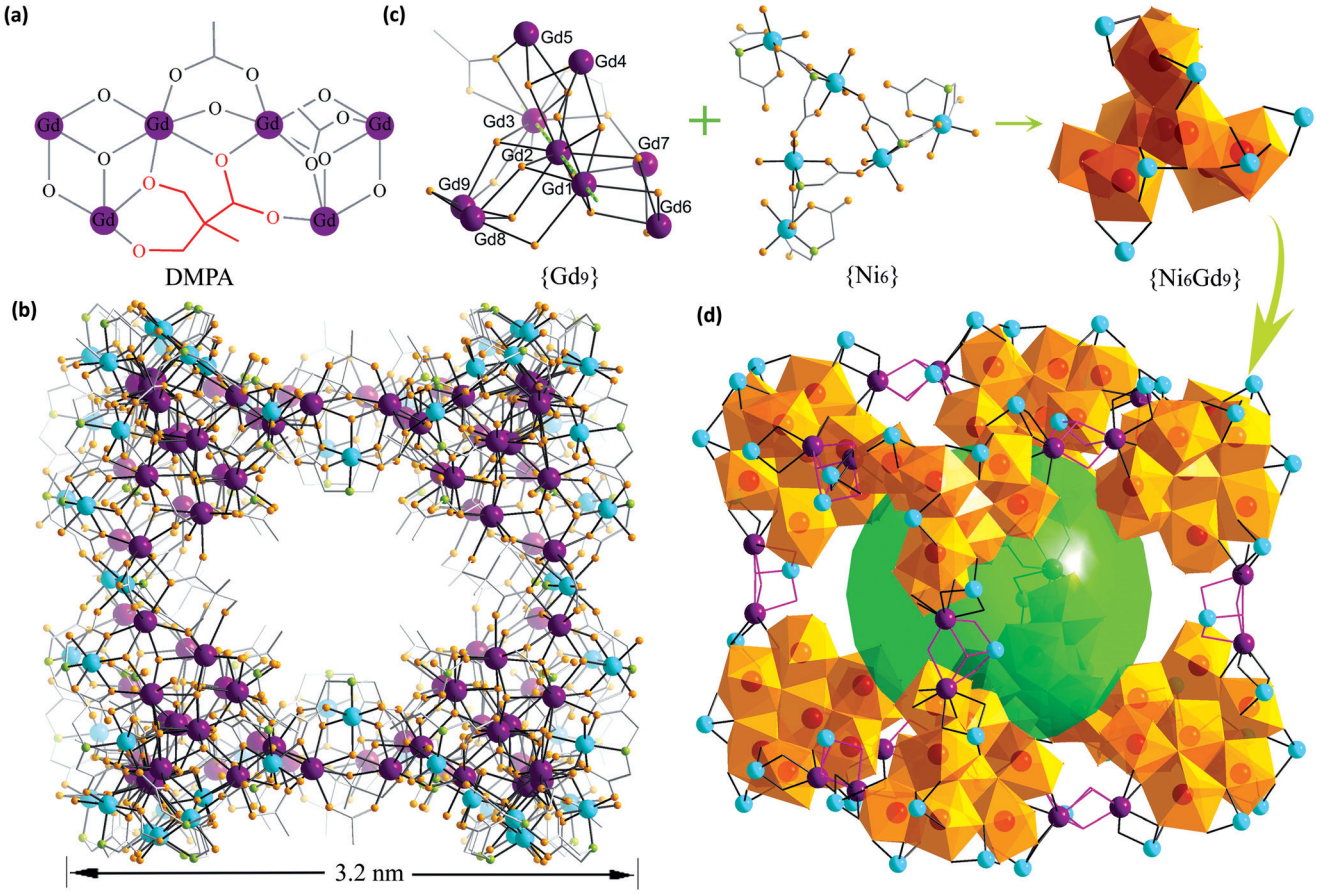

Figure 1. a) The coordination mode of the DMPA ligand. b) Ball-and-stick view of the cationic $\{Ni_{60}Gd_{96}\}$ core in **1** with H atoms removed for clarity. Gd purple, Ni cyan, N green, O orange, C gray. c) The building units of $\{Ni_{60}Gd_{96}\}$. d) The polyhedron structure of $\{Ni_{60}Gd_{96}\}$ core assembly by eight propeller-like $\{Ni_6Gd_9\}$ building units and twelve $\{NiGd_2\}$ triangular linkers. Organic ligands are removed for clarity.

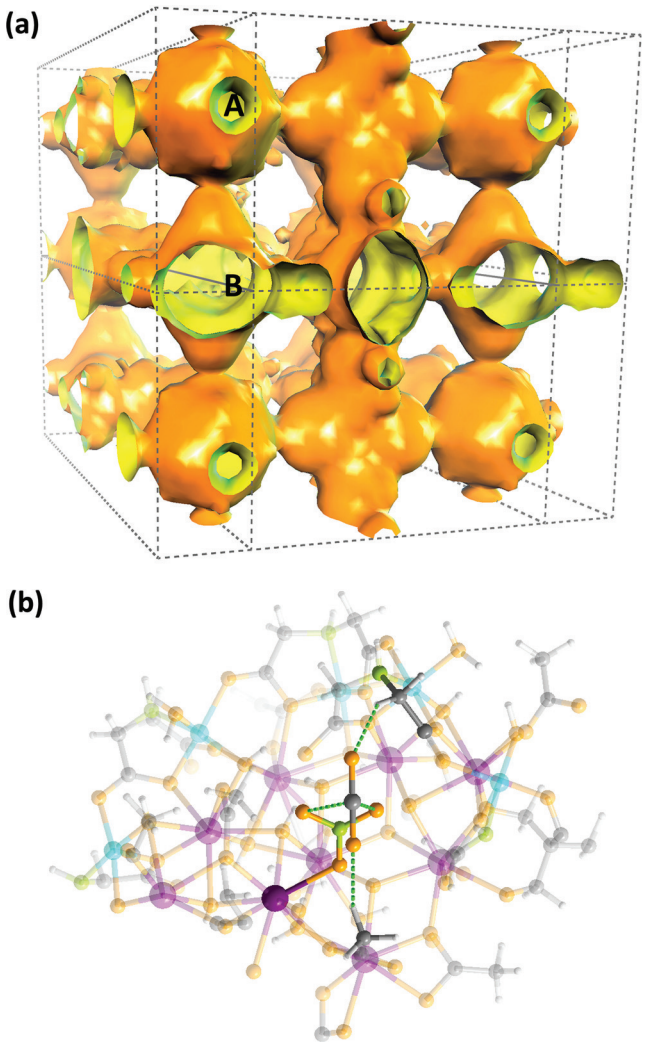

Figure 2. a) The surface view of **1**. b) Preferential adsorption site for CO_2 in **1** revealed by computational simulations. The interactions are displayed as green dashed lines. Color codes as in Figure 1.

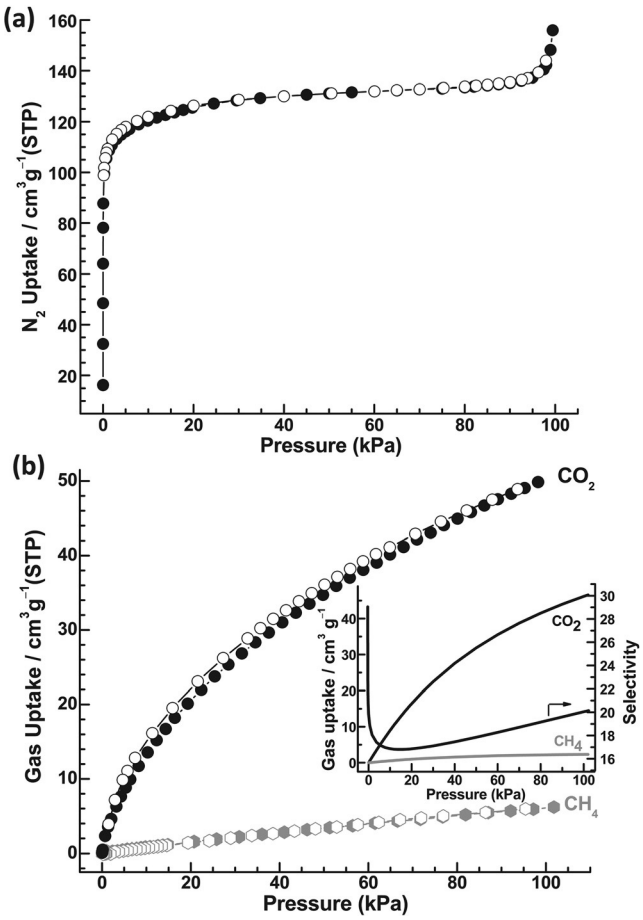

Figure 3. a) Experimental N_2 isotherms for **1** at 77 K; ● adsorption, ○ desorption. b) Adsorption isotherms of CH_4, and CO_2 at 298 K for **1**. Inset: IAST predicted selectivity for CO_2/CH_4 adsorption based on the observed adsorption isotherms of the pure gas for **1**.

sesses an inherent spherical void with an opening of 7.5 Å × 5.0 Å (Supporting Information, Figure S1 b), while cavities of B-type are formed by packing adjacent cuboidal cluster units through H-bonding interactions. As shown in the Supporting Information, Figure S5, the porous structure is a result of the alternate arrangement of the two types of cavities, which is similar to the structural features of nanoporous molecular crystals.[13]

The TGA curve of **1** (Supporting Information, Figure S7) indicates a weight loss of 10.81 % from room temperature to 150 °C because of the removal of the lattice guests (H_2O and MeOH, calcd 8.0 %) and aquo ligands (calcd 2.81 %) with decomposition starting at 250 °C. To verify the permanent porosity of the framework, a crystalline sample of **1** was completely exchanged with methanol for 36 h and then desolvated under high vacuum at 180 °C for 24 h to be activated for gas adsorption measurements. Powder X-ray diffraction (PXRD) pattern of the activated **1** corresponds well with the simulated pattern (Supporting Information, Figure S8), indicating that the structural integrity of the activated sample. The N_2 sorption isotherm of **1** measured at 77 K exhibited typical type-I characteristics, with a saturated uptake of 133 $cm^3 g^{-1}$ at STP (Figure 3), corresponding to a pore volume of 0.21 $cm^3 g^{-1}$, which is slightly lower than the value 0.24 $cm^3 g^{-1}$ calculated based on the crystal structure. The Brunauer–Emmett–Teller (BET) and Langmuir surface areas are estimated to be 467 and 610 $m^2 g^{-1}$, respectively. A pore distribution analyzed by the density functional theory (DFT) model suggests a narrow distribution of the micropores with a diameter of about 6.8 Å (Supporting Information, Figure S9), in good agreement with the metric value of Type A cavities from the crystallographic analysis (Supporting Information, Figure S1). Type B cavities have a wider pore size distribution of a 9.5–12.0 Å diameters.

Selective adsorption of CO_2 from CH_4 and N_2 is a fundamental process in CH_4 purification from natural gas. The unique cage-based porous structure prompted us to evaluate its potential application for CO_2/CH_4 and CO_2/N_2 gas separation. We measured the single-component isotherms toward CO_2 and CH_4 for **1** at 298 K by volumetric measurement. As shown in Figure 3 b, the CO_2 adsorption isotherm at 1.0 atm reaches a gas uptake of 50.0 $cm^3 g^{-1}$, which is much higher than that of CH_4 (6.2 $cm^3 g^{-1}$) under the same conditions.

From the single-component isotherms, the multi-component isotherms and the selective adsorption for CO_2/CH_4 mixture on **1** can be modeled by using the ideal adsorbed solution theory (IAST). For a mixture of equimolar CO_2 and CH_4, the selectivity of CO_2/CH_4 is in the range of 17–29 (Figure 3b, inset). Note that a material with a selectivity value of 20 at 298 K and 1.0 atm outperforms many reported MOFs under the same conditions (Supporting Information, Table S2).[14a] The N_2 adsorption isotherm at 298 K was also measured, but yielding only a small uptake (ca.1 $cm^3 g^{-1}$) at 1.0 atm (Supporting Information, Figure S10). The CO_2 and N_2 uptakes at the relevant partial pressures for flue gas (0.15 atm CO_2, 0.75 atm N_2) were also calculated to give practically useful CO_2/N_2 selectivity of 94 at 298 K. The CO_2/N_2 selectivity of **1** is also at the forefront of the list when compared with other MOFs (Supporting Information, Table S3).[14b] The highly selective adsorption of **1** for CO_2 over CH_4 or N_2 suggests its potential application for CO_2 capture from natural or flue gases.

To gain insight into the mechanism possibly responsible for the adsorption, grand canonical Monte Carlo (GCMC) simulations were employed to evaluate the interactions between the adsorbed CO_2 molecules and **1**. Preferential adsorption site and corresponding enthalpies were obtained from the simulations. The binding energy of the host–guest structure is ca. 40.1 kJ mol^{-1}, which is close to the measured value of 42 kJ mol^{-1} (Supporting Information, Figure S11). In the simulated host–guest structures, the CO_2 molecule forms two short contacts with two oxygen atoms from the same nitrate by its electropositive carbon (O···N 2.88–3.17 Å), while two oxygen atoms of CO_2 interact with one methylene group of IDA ligand and one methyl group of acetate, respectively, through two C–H···O hydrogen bonds (C···O 3.56–3.69 Å, H···O 2.55–2.76 Å, ∡C-H···N 138–146°) (Figure 2b). As such, we argue that the strong electrostatic interactions and hydrogen bonding interactions between CO_2 and framework bring about the highly selective adsorption of CO_2 over CH_4 or N_2 in **1**.

The presence of a large number of Gd^{III} ions also prompted us to investigate the magnetic properties of **1** in the context of developing molecule-based materials for magnetic cooling. Using a polycrystalline sample (Supporting Information, Figure S12), the room temperature $\chi_M T$ value of 811.2 $cm^3 K mol^{-1}$ is only slightly smaller than the calculated value of 820.0 $cm^3 K mol^{-1}$ for 64 uncorrelated Ni^{II} ions (64.0 $cm^3 K mol^{-1}$ for $S=1$ and $g=2$) and 96 uncorrelated Gd^{III} ions (756.0 $cm^3 \cdot K mol^{-1}$ for $S=7/2$ and $g=2$). Upon cooling, the $\chi_M T$ product decreases gradually, reaching a minimum of 795.8 $cm^3 K mol^{-1}$ at 36 K before increasing to a peak of 815.0 $cm^3 K mol^{-1}$ at 20 K. The up-turn of the $\chi_M T$ versus T plot below 35 K suggests a non-diamagnetic ground spin state. The χ_M^{-1} versus T plot in the temperature range of 50–300 K can be fitted well to the Curie–Weiss equation, producing $C=813.0$ $cm^3 K mol^{-1}$ and $\theta=-1.15$ K (Supporting Information, Figure S13). The negative but small Weiss constant (θ) indicates the presence of weak antiferromagnetic interactions or a combined action of spin–orbit coupling effects and weak ferromagnetic interactions among the metal centers.

The isothermal magnetization measurements for **1** were also performed from 2 to 10 K (Supporting Information, Figure S14). The M versus H curve at 2 K is under the theoretical Brillouin function for 160 uncoupled spin centers, which is consistent with the above Curie–Weiss fitting result. The magnetic entropy change ΔS_M, a parameter used to assess the magnetocaloric effect (MCE) of a material, can be calculated by the Maxwell equation $\Delta S_M(T) = \int[\partial M(T,H)/\partial T]_H dH$. The resulting ΔS_M values at different applied magnetic fields and temperatures are plotted in the Supporting Information, Figure S12 (inset); a maximum value of 42.8 J $kg^{-1} K^{-1}$ was obtained at 3 K and $\Delta H = 7$ T. This value is the largest among the values reported for transition-metal–rare-earth cluster compounds, but slightly smaller than some Gd^{III}-only clusters (Table 1).[15] The maximum entropy change calculated by using the equation $-\Delta S_M = nR\ln(2S+1)$ is $269.9R = 54.1$ J $kg^{-1} K^{-1}$. This discrepancy can be attributed to the weak magnetic interactions between the neighboring metal centers or the magnetic anisotropy originated from the Ni^{II} ions (see below).[9f]

Table 1: Reported $-\Delta S_M$ (> 35 J $kg^{-1} K^{-1}$) for reported molecules.

Complexes	$-\Delta S_M$ [J $kg^{-1} K^{-1}$]	T [K]	ΔH [T]	Ref.
$\{Gd_{104}\}$	46.9	2.0	7	[5]
$\{Gd_{24}\}$	46.1	2.5	7	[16]
$\{Gd_{48}\}$	43.6	1.8	7	[17]
$\{Ni^{II}_{64}Gd^{III}_{96}\}$ (**1**)	42.8	3.0	7	this work
$\{Co^{II}_{9}Co^{III}Gd^{III}_{42}\}$	41.3	2.0	7	[11a]
$\{Gd_2\}$	40.6	1.8	7	[18]
$\{Ni^{II}_{10}Gd^{III}_{42}\}$	38.2	2.0	7	[11a]
$\{Gd_{38}\}$	37.9	1.8	7	[19]
$\{Ni^{II}_{12}Gd^{III}_{36}\}$	36.3	3.0	7	[11b]
$\{Gd_{12}\}$	35.3	3.0	7	[20]

The significance of Gd^{III} in compounds with large MCEs is commonly accepted, but systems offering the opportunity to pin down the critical contribution of Gd^{III} are not readily available unless 3d or 4f metals in a heterometallic compound can be substituted for diamagnetic metal ions. We were able to obtain the isostructural compound **3** in which diamagnetic Y(III) ions are present in place of Gd^{III} in **1**. Comparative magnetic studies (Supporting Information, Figures S15 and S16) were carried out under otherwise identical conditions for **3**. The $\chi_M T$ product remains nearly constant until 35 K and then increases gradually to a maximum value of 64.6 $cm^3 K mol^{-1}$ at 7.5 K. The χ_M^{-1} versus T plot in 50–300 K obeys the Curie–Weiss law with $C=63.6$ $cm^3 K mol^{-1}$ and $\theta=-0.3$ K. In contrast to **1**, the reduced Weiss constant presumably indicates weak ferromagnetic interactions among the Ni^{II} centers, which may compete with the spin–orbit coupling effects of the single nickel(II) ions or antiferromagnetic interactions with other metal centers. The calculated maximum MCE for **3** is only 9.2 J $kg^{-1} K^{-1}$. It becomes clear that the large MCE in **1** arises primarily from the Gd^{III} ions (Supporting Information, Figure S17). However, owing to the complexity of the system, quantitative analysis of the magnetic couplings between the metal centers is practically impossible.

Ac susceptibility data of **1**–**3** (Supporting Information, Figures S18–S20) reveal no single-molecule magnet behavior down to 2 K. MCE studies for **2** also show much less entropy change ($-\Delta S_{Max} = 18.9\ J\,kg^{-1}\,K^{-1}$ at 4 K and $H = 7$ T) as compared to **1**, which further confirm the significant contribution of Gd^{III} ions to large MCE in **1** (Supporting Information, Figures S21 and S22).

In summary, we have obtained the highest-nuclearity heterometallic transition-metal–rare-earth cluster complexes by using organic ligands of distinct coordination characteristics. Such porous cages are robust and exhibit fantastic function of high selective gas adsorption of CO_2 over CH_4 or over N_2 at room temperatures. The presence of a large number of interesting magnetically metal ions in an integrated molecular platform offers the opportunity to study how different metal ions contribute to bring about the interesting properties that are useful in developing molecular functional materials. Finally, we expect that this mixed-ligand approach to be quite general in facilitating the assembly of cluster motifs whose structures are complex and aesthetically pleasing but cannot be predicted a priori based merely on ligand structures.

Acknowledgements

This work was supported by NSFC (21473129), "National Young 1000-Plan" program and Wuhan National High Magnetic Field Center (2015KF06). We are grateful for Prof. Dr. Jie-Peng Zhang (Sun Yat-Sen University) and Dr. Yanyan Wang for significant discussions.

Keywords: cluster complexes · coordination cages · gas separation · magnetic cooling · rare-earth elements

How to cite: *Angew. Chem. Int. Ed.* **2016**, *55*, 9375–9379
Angew. Chem. **2016**, *128*, 9521–9525

[1] C. Papatriantafyllopoulou, E. E. Moushi, G. Christou, A. J. Tasiopoulos, *Chem. Soc. Rev.* **2016**, *45*, 1597–1628.
[2] A. Müller, E. Beckmann, H. Bögge, M. Schmidtmann, A. Dress, *Angew. Chem. Int. Ed.* **2002**, *41*, 1162–1167; *Angew. Chem.* **2002**, *114*, 1210–1215.
[3] C. E. Anson, A. Eichhöfer, I. Issac, D. Fenske, O. Fuhr, P. Sevillano, C. Persau, D. Stalke, J. Zhang, *Angew. Chem. Int. Ed.* **2008**, *47*, 1326–1331; *Angew. Chem.* **2008**, *120*, 1346–1351.
[4] N. T. Tran, D. R. Powell, L. F. Dahl, *Angew. Chem. Int. Ed.* **2000**, *39*, 4121–4125; *Angew. Chem.* **2000**, *112*, 4287–4291.
[5] J.-B. Peng, X.-J. Kong, Q.-C. Zhang, M. Orendáč, J. Prokleška, Y.-P. Ren, L.-S. Long, Z. Zheng, L.-S. Zheng, *J. Am. Chem. Soc.* **2014**, *136*, 17938–17941.
[6] G. E. Sigmon, D. K. Unruh, J. Ling, B. Weaver, M. Ward, L. Pressprich, A. Simonetti, P. C. Burns, *Angew. Chem. Int. Ed.* **2009**, *48*, 2737–2740; *Angew. Chem.* **2009**, *121*, 2775–2778.
[7] A. J. Tasiopoulos, A. Vinslava, W. Wernsdorfer, K. A. Abboud, G. Christou, *Angew. Chem. Int. Ed.* **2004**, *43*, 2117–2121; *Angew. Chem.* **2004**, *116*, 2169–2173.
[8] a) A. Müller, P. Gouzerh, *Chem. Soc. Rev.* **2012**, *41*, 7431–7463; b) A. Schnepf, *Chem. Soc. Rev.* **2007**, *36*, 745–758; c) H. Schnöckel, *Chem. Rev.* **2010**, *110*, 4125–4163; d) G. Li, Z. Lei, Q.-M. Wang, *J. Am. Chem. Soc.* **2010**, *132*, 17678–17679; e) A. Dass, S. Theivendran, P. R. Nimmala, C. Kumara, V. R. Jupally, A. Fortunelli, L. Sementa, G. Barcaro, X. Zuo, B. C. Noll, *J. Am. Chem. Soc.* **2015**, *137*, 4610–4613.
[9] a) R. Ahlrichs, A. Eichhöfer, D. Fenske, O. Hampe, M. M. Kappes, P. Nava, J. Olkowska-Oetzel, *Angew. Chem. Int. Ed.* **2004**, *43*, 3823–3827; *Angew. Chem.* **2004**, *116*, 3911–3915; b) Y. Liu, B. K. Najafabadi, M. A. Fard, J. F. Corrigan, *Angew. Chem. Int. Ed.* **2015**, *54*, 4832–4835; *Angew. Chem.* **2015**, *127*, 4914–4917; c) H. Yang, Y. Wang, H. Huang, L. Gell, L. Lehtovaara, S. Malola, H. Häkkinen, N. Zheng, *Nat. Commun.* **2013**, *4*, 1–8; d) H. Yang, Y. Wang, J. Yan, X. Chen, X. Zhang, H. Häkkinen, N. Zheng, *J. Am. Chem. Soc.* **2014**, *136*, 7197–7200; e) H. Yang, Y. Wang, J. Lei, L. Shi, X. Wu, V. Makinen, S. C. Lin, Z. Tang, J. He, H. Hakkinen, L. Zheng, N. Zheng, *J. Am. Chem. Soc.* **2013**, *135*, 9568–9571; f) Y.-Z. Zheng, G.-J. Zhou, Z. Zheng, R. E. P. Winpenny, *Chem. Soc. Rev.* **2014**, *43*, 1462–1475.
[10] a) Y.-Z. Zheng, M. Evangelisti, R. E. P. Winpenny, *Chem. Sci.* **2011**, *2*, 99–102; b) Y.-Z. Zheng, M. Evangelisti, R. E. P. Winpenny, *Angew. Chem. Int. Ed.* **2011**, *50*, 3692–3695; *Angew. Chem.* **2011**, *123*, 3776–3779; c) Y.-Z. Zheng, M. Evangelisti, F. Tuna, R. E. P. Winpenny, *J. Am. Chem. Soc.* **2012**, *134*, 1057–1065; d) Y.-Z. Zheng, E. M. Pineda, M. Helliwell, R. E. P. Winpenny, *Chem. Eur. J.* **2012**, *18*, 4161–4165.
[11] a) X.-J. Kong, Y.-P. Ren, L.-S. Long, Z. Zheng, R.-B. Huang, L.-S. Zheng, *J. Am. Chem. Soc.* **2007**, *129*, 7016–7017; b) X.-J. Kong, Y.-P. Ren, W.-X. Chen, L.-S. Long, Z. Zheng, R.-B. Huang, L.-S. Zheng, *Angew. Chem. Int. Ed.* **2008**, *47*, 2398–2401; *Angew. Chem.* **2008**, *120*, 2432–2435; c) X.-J. Kong, L.-S. Long, R.-B. Huang, L.-S. Zheng, T. D. Harris, Z. Zheng, *Chem. Commun.* **2009**, 4354–4356.
[12] Crystal data for **1**: $Ni_{64}Gd_{96}C_{447}H_{1212}N_{88}O_{847}Cl_{24}$, $M_r = 41077$, monoclinic, space group $C2/m$, $a = 65.583(7)$ Å, $b = 34.422(4)$ Å, $c = 34.062$ (4) Å, $\beta = 110.548(5)$, $V = 72004(14)$ Å^3, $Z = 2$. Mo-Kα radiation ($\lambda = 0.71073$ Å), $T = 150$ K, $\mu = 5.30\ mm^{-1}$, $R_1 = 0.065$, $wR_2 = 0.191$ for 49383 observed reflections from 64579 independent reflections, GOF = 1.15. CCDC 1034661 (**1**), 1402448 (**2**) and 1034662 (**3**) contain the supplementary crystallographic data for this paper. These data can be obtained free of charge from The Cambridge Crystallographic Data Centre.
[13] N. B. McKeown, *J. Mater. Chem.* **2010**, *20*, 10588–10597.
[14] a) J.-R. Li, Y. Ma, M. C. McCarthy, J. Sculley, J. Yu, H.-K. Jeong, P. B. Balbuena, H.-C. Zhou, *Coord. Chem. Rev.* **2011**, *255*, 1791–1823; b) K. Sumida, D. L. Rogow, J. A. Mason, T. M. McDonald, E. D. Bloch, Z. R. Herm, T. H. Bae, J. R. Long, *Chem. Rev.* **2012**, *112*, 724–781.
[15] J.-L. Liu, Y.-C. Chen, F.-S. Guo, M.-L. Tong, *Coord. Chem. Rev.* **2014**, *281*, 26–49.
[16] L.-X. Chang, G. Xiong, L. Wang, P. Cheng, B. Zhao, *Chem. Commun.* **2013**, *49*, 1055–1057.
[17] F.-S. Guo, Y.-C. Chen, L.-L. Mao, W.-Q. Lin, J.-D. Leng, R. Tarasenko, M. Orendáč, J. Prokleška, V. Sechovský, M.-L. Tong, *Chem. Eur. J.* **2013**, *19*, 14876–14885.
[18] M. Evangelisti, O. Roubeau, E. Palacios, A. Camín, T. N. Hooper, E. K. Brechin, J. J. Alonso, *Angew. Chem. Int. Ed.* **2011**, *50*, 6606–6609; *Angew. Chem.* **2011**, *123*, 6736–6739.
[19] M.-Y. Wu, F.-L. Jiang, X.-J. Kong, D.-Q. Yuan, L.-S. Long, S. A. Al-Thabaiti, M.-C. Hong, *Chem. Sci.* **2013**, *4*, 3104–3109.
[20] Y. Zheng, Q.-C. Zhang, L.-S. Long, R.-B. Huang, A. Müller, J. Schnack, L.-S. Zheng, Z. Zheng, *Chem. Commun.* **2013**, *49*, 36–38.

Received: April 22, 2016
Published online: June 27, 2016

